On localized vegetation patterns, fairy circles and localized patches in arid landscapes

D. Escaff[1], C. Fernandez-Oto[2], M.G. Clerc[3] and M. Tlidi[2]

[1]*Complex Systems Group, Facultad de Ingeniería y Ciencias Aplicadas,*
Universidad de los Andes, Monseñor Alvaro del Portillo 12.455, Las Condes, Santiago, Chile,
[2]*Faculté des Sciences, Université Libre de Bruxelles (U.L.B.),*
C.P. 231, Campus Plaine, B-1050 Bruxelles, Belgium and
[3]*Departamento de Física, Universidad de Chile, Blanco Encalada 2008, Santiago, Chile.*

We investigate the formation of localized structures with a varying width in one and two-dimensional systems. The mechanism of stabilization is attributed to strong nonlocal coupling mediated by a Lorentzian type of Kernel. We show that, in addition to stable dips found recently [see, e.g., C. Fernandez-Oto, M. G. Clerc, D. Escaff, and M. Tlidi, Phys. Rev. Lett. **110**, 174101 (2013)], exist stable localized peaks which appear as a result of strong nonlocal coupling, i.e. mediated by a coupling that decays with the distance slower than an exponential. We applied this mechanism to arid ecosystems by considering a prototype model of a Nagumo type. In one-dimension, we study the front that connects the stable uniformly vegetated state with the bare one under the effect of strong nonlocal coupling. We show that strong nonlocal coupling stabilizes both—dip and peak—localized structures. We show analytically and numerically that the width of localized dip, which we interpret as fairy circle, increases strongly with the aridity parameter. This prediction is in agreement with filed observations. In addition, we predict that the width of localized patch decreases with the degree of aridity. Numerical results are in close agreement with analytical predictions.

PACS numbers:

I. INTRODUCTION

Localized structures (LS's) in dissipative media have been observed in various field of nonlinear science such as fluid dynamics, optics, laser physics, chemistry, and plant ecology (see recent overviews [1, 2]). Localized structures consist of isolated or randomly distributed spots surrounded by regions in the uniform state. They may consist of dips embedded in the homogeneous background. They are often called spatial solitons, dissipative solitons, localized patterns, cavity solitons, or auto-solitons depending on the physical contexts in which their were observed. Localized structures can occur either in the presence [3] or in the absence [4] of a symmetry breaking instability. In the last case, bistability between uniform states is a prerequisite condition for LS's formation. However, in the presence of symmetry breaking instability, the coexistence between a single uniform solution and a patterned state allows for the stabilization of LS's [4]. In this case, bistability condition between uniform solutions is not a necessary condition for generating LS's [5].

Spatial coupling in many spatially extended systems is nonlocal. The Kernel function that characterizes the nonlocality can be either weak and strong. If the Kernel function decays asymptotically to infinity slower than an exponential function, the nonlocal coupling is said to be strong [6]. If the Kernel function decays asymptotically to infinity faster than an exponential function, the nonlocal coupling is said to be weak. Self-organization phenomenon leading to the formation of either extended or localized patterns under a local and nonlocal coupling occur in various systems such as fluid dynamics [7], firing of cells [8, 9], propagation of infectious diseases [10], chemical reactions [11, 12], population dynamics [13–15], nonlinear optics [16–22], granular [23], and vegetation patterns [24–28].

We focus on bistable regime far from any symmetry breaking instability, i.e. far from any Turing instability. In this case, the behavior of many systems is governed by front dynamics or domains between the homogeneous steady states. When the nonlocal coupling is weak, the interaction between two fronts is usually described by the behavior of the tail of fronts. However, for strong nonlocal coupling, the interaction is controlled by the whole Kernel function and not by the asymptotic behavior of the front tails [6].

When a non-local coupling is weak, the asymptotic behavior of front solutions is characterized by exponential decay or damping oscillations. In the former case, front interaction is always attractive and decays exponentially with the distance between the fronts. In two dimensional setting, LS's resulting from fronts interaction are unstable. In the case of damping oscillations, front interactions alternate between attractive and repulsive with an intensity that decays exponentially with the distance between the two fronts [29]. For a fixed value of parameters, a family of stable one dimensional localized structures with different sizes has been reported in [13, 30–32]. An important difference appears when considering a strong nonlocal coupling. This difference is that the interaction between fronts can be repulsive [33, 34].

Strong nonlocal coupling has been observed experimentally in various systems. Indeed, several experimental mea-
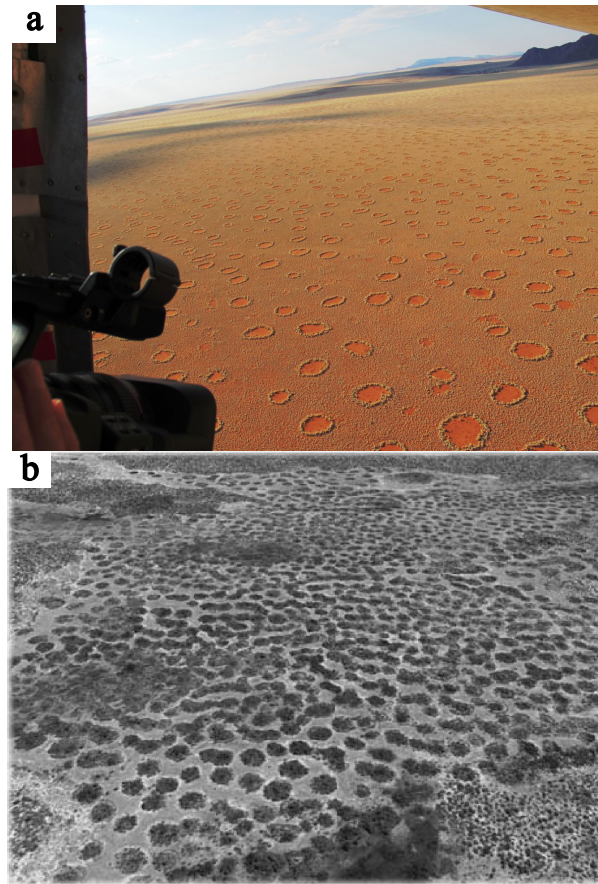
Figure 1: (Color online) Localized vegetation patterns: (a) An aerial photo taken on 05 March 2010 shows fairy circles in the Namibrand region, Namibia. Image courtesy of Professor Norbert Juergens. (b) An aerial photograph showing localized vegetation patches, Zambia [61].

surements of nonlocal response in the form of Lorentzian or a generalized Lorentzian have been carried out in nematic liquid crystals cells [36, 37]. Experimental reconstruction of strong nonlocal coupling has also been performed in photorefractive materials [38]. In this case, the strong nonlocal coupling is originating from the thermal medium effects. In population dynamics such as vegetation, it has been shown experimentally that seed dispersion may be described by a Lorentzian [39].

We consider a proto model for population dynamics, namely the strong nonlocal Nagumo equation [33]. This model possesses two relevant properties: strong nonlocal coupling and bistability between uniformly vegetated and bare states. We focus on a regime far from any symmetry breaking or Turing type of instabilities. In this regime localized structures resulting from strong nonlocal coupling can be stabilized in a wide range of parameters [33]. We will investigate two types of localized vegetation structures: i) isolated or randomly distributed circular areas devoid of any vegetation, often called fairy circles (FC's), and ii) isolated or randomly distributed circular areas of vegetation, surrounded by a bare region. An example of FC's is shown in an areal photograph (see Fig. 1a). They are observed in vast territories in southern Angola, Namibia, and South Africa [40–48]. The size of these circles can reach diameters of up to 12m. An in-depth investigation of several hypotheses concerning their origin has been performed by van Rooyen et al. [49]. In this study, these authors have been able to excluded the possible existence radioactive areas inapt for the development of plants, the termites activity and the release of allelopathic compounds. We attribute two main ingredients to their stabilization: the bistability between the bare state and the uniformly vegetation state, and Lorentzian-like non-local coupling that models the competition between plants [34]. We provide detailed analysis of the fairy circle formation in a simple population dynamics model. In addition we show that the above mechanism applies to another type of localized structures that consist of isolated or randomly distributed vegetation patches surrounded by a bare state. An example of this behavior is shown in Fig. 1b. In this paper, we investigate analytically and numerically the formation of both—fairy circles and localized patches–and their existence range. Our theoretical analysis shows that exist a Maxwell point above which localized patches are stable, while below

this point fairy circles appear. Finally, we investigate how the degree of aridity affects the width of both types of localized vegetation structures.

This paper is organized as follows. After a briefly introducing the model describing the vegetation dynamics, namely the Nagumo model with strong nonlocal coupling mediated by a Lorentzian function (Sec. II). We describe the dynamics of a single front in one dimension, and its asymptotic behaviors (Sec. III). The analytical and numerical analysis of the interaction between fronts connecting the uniformly vegetated and the bare steady states is described in Sec. IV, where we discuss the formation of both fairy circles and localized patches. Close to the Maxwell point, we derive a formula for the width of both localized structures as a function of the degree of the aridity in one dimension. We conclude in Sec. V.

II. THE NAGUMO MODEL

Several models describing vegetation patterns and self-organization in arid and semiarid landscapes have been proposed during last two decades. They can be classified into three types. The first approach is based on the relationship between the structure of individual plants and the facilitation-competition interactions existing within plant communities [24–26, 50, 51]. The second is based on the reaction-diffusion approach which takes into account of the influence of water transport by below ground diffusion and/or above ground run-off [52–58]. The third approach focuses on the role of environmental randomness as a source of noise induced symmetry breaking transitions [59–62]. Recently, the reduction of a generic interaction-redistribution model, which belong to the first class of ecological type of models [26], to a Nagumo-type model has been established [34]. Here, we consider the variational nonlocal Nagumo-type equation

$$\partial_t u = u(\alpha - u)(u - 1) + \nabla^2 u + \epsilon u \int_\Omega u^2(\mathbf{r} + \mathbf{r}', t) K(\mathbf{r}') d\mathbf{r}' \tag{1}$$

where $u(\mathbf{r}, t)$ is a normalized scalar field that represents the population density or biomass, α is a parameter describing the environment adversity or the degree of aridity, t is time. We consider that population or plant community established on a spatially uniform territory Ω. The vegetation spatial propagation, via seed dispersion and/or other natural mechanisms, is usually modeled by a non-local coupling with a Gaussian like Kernel [24–26]. For simplicity, we consider only the first term in Taylor expansion of the dispersion. This approximation leads to the Laplace operator, $\nabla^2 = \partial_{xx} + \partial_{yy}$ acting in the space $\mathbf{r} = (x, y)$. The last term in Eq. 1 describes the competitive interaction between individual plants through their roots. The nonlocal coupling intensity, denoted by ϵ, should be positive to ensure a competitive interaction between plants. The kernel function has the form $K(\mathbf{r}) = \delta(\mathbf{r}) - f_\sigma(\mathbf{r})$, where $\delta(\mathbf{r})$ is the delta function. The inclusion of the δ function in the analysis allows us to avoid the variation of the spatially uniform states as a function the nonlocal intensity ϵ, and

$$f_\sigma(\mathbf{r}) = \frac{N_n}{1 + (|\mathbf{r}|/\sigma)^n}, \tag{2}$$

which has an effective range σ. For the sake of simplicity, we consider that the length σ is a constant, independent of the biomass. Hence, we assume all plants have the same root size, that is, we neglect allometric effect [50, 63]. At large distance, the asymptotic behavior of the Kernel is determined by n, and N_n is normalization constant.

It is worth to emphasize that, since the strong nonlocal term in Eq. (1) models the interaction between individual plants at the community level , we refer to it as strong nonlocal interaction or coupling. In contrast, non-localities describing transport processes, as seed dispersion [24–26], for sake of simplicity, we are modeling by the Laplace operator.

The Eq. (1) is variational and it is described by

$$\partial_t u = -\frac{\delta \mathcal{F}}{\delta u} \Rightarrow \frac{d\mathcal{F}}{dt} \leq 0, \tag{3}$$

where $\mathcal{F}$ is a Lyaponov functional that can only decrease in the course of time. Accordingly, any initial distribution $u(\vec{r}, t)$ evolves towards a homogeneous or inhomogeneous (periodic or localized) state corresponding to a local or global minimum of $\mathcal{F}$. The Lyaponov functional reads

$$\mathcal{F}[u] = \int_\Omega \left\{ \frac{1}{2}(|\nabla u|^2 + V(u) \right\} dr$$
$$+ \frac{\epsilon}{4} \int_\Omega \int_\Omega u^2(\mathbf{r}) u^2(\mathbf{r}') K(\mathbf{r} - \mathbf{r}') dr dr'$$

and

$$V\left(u\right) = \frac{u^2}{4}\left(u - 1\right)^2 + \frac{u^2}{6}\left(\alpha - 1/2\right)\left(3 - 2u\right). \tag{4}$$

The Eq. (1) admits three spatially uniform solutions $u = 0$, $u = \alpha$ and $u = 1$. The bare state $u = 0$ is always stable, and represents not plant state. The uniform state $u = \alpha$ is always unstable. For large values of α, the climate becomes more and more arid. The uniformly vegetated state $u = 1$ may undergo a may undergo a symmetry breaking type of instability (often called Turing instability), that leads to pattern formation. In one dimensional system, and for $n = 2$, the threshold for that instability satisfies

$$\beta = \epsilon \sigma^2 \exp(-\beta), \tag{5}$$

with $\beta = \sqrt{1 + \sigma^2(2\epsilon + \alpha - 1)} - 1$. In what follows, we will focus on a regime far from any pattern forming instability.

III. FRONTS

We consider a bistable regime where $u = 0$ and $u = 1$ are both linearly stable. From Eq. (4), $V\left(0\right) = 0$ and $V\left(1\right) = \left(\alpha - 1/2\right)/6$. Therefore, when $\alpha < 1/2$, the most favorable state is the uniformly vegetated one. When $\alpha > 1/2$, the bare state is more stable than the uniformly vegetated one. There exist a particular point where both states are equally stable. This point is usually called the Maxwell point [35], and corresponds to $\alpha = 1/2$.

Depending on the value of α, front connecting both state will propagate towards the most stable state. An example of a single front is illustrated in Fig. 2.a. The time-space diagram of Fig. 2.b shows how the most stable state, corresponding to the bare state $(\alpha > 1/2)$, invades the uniformly vegetated state, with a constant speed. Fronts propagate following the minimization of the potential (4) and the front velocity is proportional to the energy difference between equilibria $V\left(1\right) - V\left(0\right)$. The front is motionless at the Maxwell point for $\alpha = 1/2$. At this point and in the absence of nonlocal coupling, $\epsilon = 0$, front solutions read

$$u_{\pm}\left(x - x_0\right) = \frac{1}{2}\left(1 \pm \tanh\left(\frac{x - x_0}{2\sqrt{2}}\right)\right), \tag{6}$$

where x_0 corresponds to the interphase position. The front u_+ links the barren state from $x = -\infty$ to the uniformly vegetated state at $x = \infty$. The opposite connection correspond to u_-.

The asymptotic behavior of the front solutions (6) obeys to an exponential law in the form

$$u_+\left(x \ll x_0\right) \approx e^{(x-x_0)/\sqrt{2}},$$
$$u_+\left(x \gg x_0\right) \approx 1 - e^{-(x-x_0)/\sqrt{2}}.$$

Around the barren state $(u = 0)$, the inclusion of the nonlocal interaction does not modify the asymptotic behavior of the front, since the nonlocality in model (1) is nonlinear. Let us examine the effect of nonlocal term around the uniformly vegetated steady state $(u = 1)$. For this purpose, let us assume that the asymptotic behavior of the front obeys to an exponential law in the form

$$u\left(x \gg x_0\right) \approx 1 - ce^{-\lambda(x-x_0)},$$

where c is a constant, and the exponent λ obeys the equation

$$\lambda^2 - \frac{1}{2} + \epsilon\left(3 - 2g_\sigma\left(\lambda\right)\right) = 0,$$

where

$$g_\sigma\left(\lambda\right) = \int_{-\infty}^{\infty} \cosh\left(\lambda x\right) f_\sigma\left(x\right) dx.$$

This equation has been successfully used to explain the emergence of localized domains. When λ-solutions have non-null imaginary part, spatially damped oscillations on the front profile are induced, leading to the stabilization of localized domain. This mechanism is well documented for either local or nonlocal systems [13, 30, 31, 64].

The g_σ function exists when the Kernel decays faster than an exponential one, i.e., a weak nonlocal coupling. In the case of strong nonlocal interaction, g_σ diverges and the above analysis is no more longer valid.
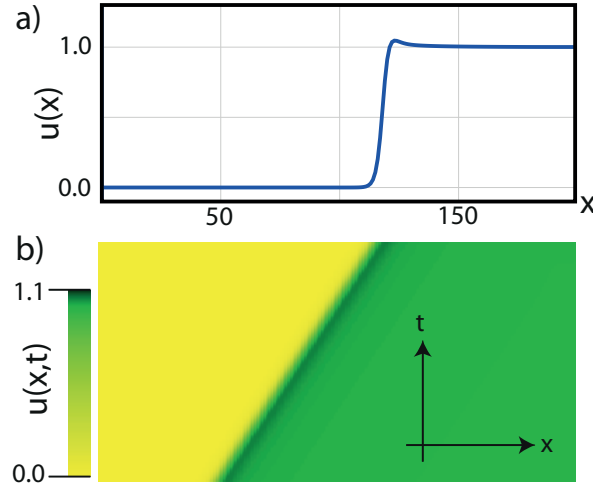
Figure 2: (Color online) Front propagation obtained from numerical simulations of Eq. (1). (a) Biomass front profile. (b) Spatiotemporal diagram that shows the front movement with a constant speed. The parameters are $\alpha = 0.51$, $\sigma = 0.7$, $n = 2$ and $\epsilon = 1.0$.

To determine the asymptotic behavior of the front around the uniformly vegetated state under strong nonlocal coupling, we perform a regular perturbation analysis in terms of small parameter ϵ. At the Maxwell point, we expand the field as

$$u(x) = u_0(x) + \epsilon u_1(x) + \epsilon^2 u_2(x) + ...,\tag{7}$$

where $u_0 = u_+$ is the motionless front provided by the Eq. (6). Replacing (7) in Eq.(1), and making an expansion in series of ϵ. At order ϵ, we obtain:

$$\{\partial_{xx} - 1/2 + 3u_0(1 - u_0)\}u_1 =$$
$$\left(u_0 \int_{-\infty}^{\infty} u_0^2(x + x')f_\sigma(x')dx' - u_0^3\right).$$

Let us focus in the region $x \gg x_0$, and neglecting all exponential corrections coming from u_0, then we obtain

$$\{\partial_{xx} - 1/2\}u_1 = -\int_{x-x_0}^{\infty} f_\sigma(x')\,dx'.\tag{8}$$

Equation (8) is a linear inhomogeneous equation for the correction u_1. For strong nonlocal coupling, the particular solution of Eq. 8 dominates over the homogeneous one which is exponentially small. For instance, if we consider a Kernel like

$$f_\sigma(x) \approx \frac{N}{x^n} \quad \text{for} \quad x \gg 1,\tag{9}$$

with $n > 1$ and N a normalization constant. For $x - x_0 \gg 1$, the front approaches asymptotically the following solution

$$u \approx 1 + \frac{2\epsilon N}{(n-1)(x - x_0)^{n-1}}.\tag{10}$$

This solution decays according to a power law $1 - n$. To check the power obtained from the above analysis, we perform a numerical simulations of the full model Eq. (1). The result obtained from Eq. (9) and the numerical simulations are shown in in Fig. 3. Both results agree perfectly without any adjusting parameter. Note that both analytical calculations and numerical simulations predict the existence of one peak in the spatial profile of the front. This peak takes place at the interface separating both homogeneous steady states as shown in Fig. 3.
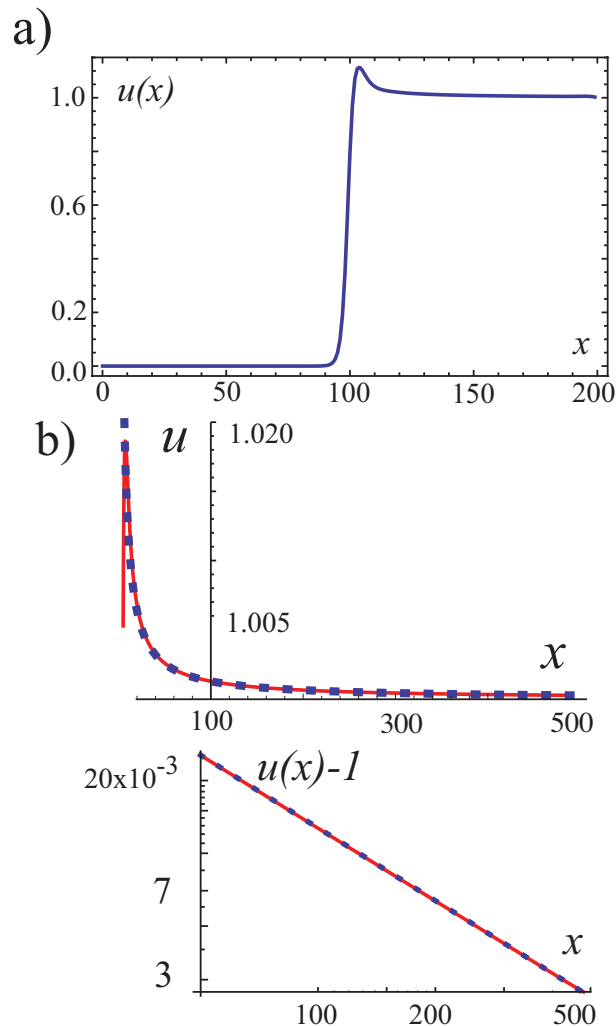
Figure 3: (Color online) Numerical solutions of model (1), with the Lorentzian kernel (2). (a) Front profile at the Maxwell point $\alpha = 0.5$, other parameters are $\sigma = 2$, $n = 2$ and $\epsilon = 0.35$. (b) Decay of front to the uniformly vegetated state for $\alpha = 0.5$, $\sigma = 2$, $n = 2$ and $\epsilon = 0.1$. In (b), the upper panel shows the comparison between the numerical calculation (dotted line) and the analytical estimation (10) (continuous line), while the lower panel displays the same comparison in a log-log plot.

IV.   LOCALIZED VEGETATION PATTERNS

Far from a symmetry breaking instability, localized structures can be stable as a results of front interactions. This phenomenon occurs when the spatial profile of the front exhibits damped oscillations [13, 64]. However, around the bare state damped oscillations are nonphysical since the biomass is a positive defined quantity. A stabilization mechanism of LS's based on combined influence of strong nonlocal coupling and bistability has been proposed [33]. This mechanism has been applied to explain the origin of the fairy circles phenomenon in realistic ecological model [34]. To the best our knowledge, there is no other analytical understanding of the circular shape of the fairy circle. We have shown in addition that the diameter of the single fairy circle is intrinsic to the dynamics of the system such as the competitive interaction between plant and the redistribution of resources [34]. We believe that extrinsic causes such as termite or ant or others external environment cannot explain the circular shape of fairy circles.

In this section we provide a detailed analysis of front interactions leading to stabilization of both fairy circles and localized patches. For both types of localized vegetation structures, we discuss how the level of aridity affects their diameter.
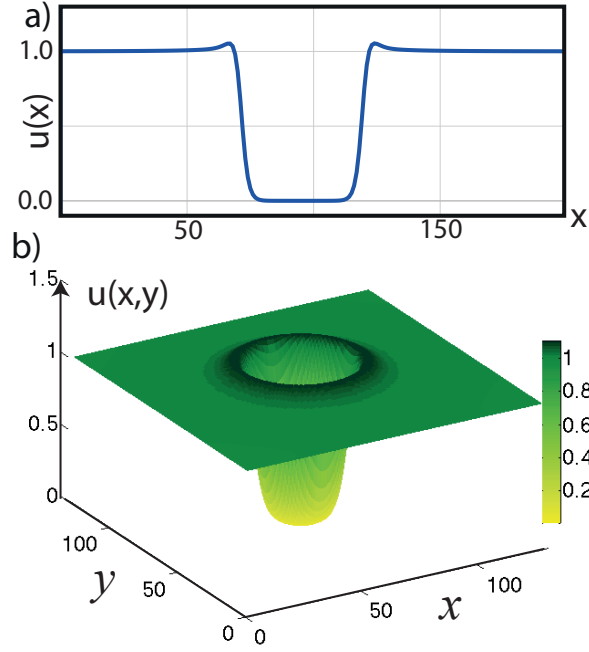
Figure 4: (Color online) Stationary fairy circle obtained from numerical simulations of Eq. (1). (a) One dimension with $\alpha = 0.492$, $\sigma = 0.8$, $n = 2$ and $\epsilon = 0.5$. (b) Two dimensions with $\alpha = 0.38$, $\sigma = 0.2$, $n = 2.2$ and $\epsilon = 1$.

A.   Fairy circles

The model Eq. (1) admits stable localized structures in the form of bare state embedded in herbaceous vegetation matrix. An example of such behavior is shows in Fig. 4. They are stable and permanent structures. A single fairy circle exhibits a fringe formed by tall grass that separate the bare state to the uniformly vegetated as shown in Fig. 1a. From numerical simulations, we see that the biomass possess one peak that takes place in between the bare and the uniformly vegetated states as shows in Fig. 4. This can be explain by the fact that inside the circle the competition between plant is small. Indeed the length of the plant root is much smaller than the diameter of the fairy circle.

We analytically investigate the formation of a single fairy circle in one spatial dimension. We focus on the parameter region near to Maxwell point ($\frac{1}{2} - \alpha = \eta \ll 1$) and we consider a small non-local coupling ($\epsilon \ll 1$). We look for a solution of Eq. (1) that has the form of a slightly perturbed linear superposition of two fronts

$$u(x,t) = u_+ \left(x - \delta(t) \right) + u_- \left(x + \delta(t) \right) + W, \tag{11}$$

where $W(x, u_+, u_-)$, $\partial_t \delta$, η and ϵ are small in a sense that will be pinned down bellow. While $u_\pm$ are defined by Eq. (6).

Replacing anstatz (11) in Eq. (1) and neglecting high order terms in ϵ, we obtain

$$- (\partial_x u_+ - \partial_x u_-) \partial_t \delta = u_+ u_- (3 - 3u_+ - 3u_-)$$
$$+ \epsilon u \int_{-\infty}^{\infty} u^2(x + x', t) K(x') dx'$$
$$- \eta(u_+ + u_- - 1)(u_+ + u_-) + LW + h.o.t., \tag{12}$$

where the linear operator L has the form

$$L \equiv -\frac{1}{2} + 3u_+ - 3u_+^2 + \partial_{xx} + 3u_- - 3u_-^2 - 6u_+ u_-.$$

To solve the above equation, we consider the inner product $\langle g|h \rangle \equiv \int_{-\infty}^{+\infty} (g(x)h(x))dx$. Then, the linear operator L_+ is self-adjoint and $L\partial_x u_\pm \approx 0$. The solvability condition gives

$$- \langle \partial_x u_+ | \partial_x u_+ \rangle \, \partial_t \delta = G + \eta \langle \partial_x u_+ | (1 - u_+) u_+ \rangle , \tag{13}$$
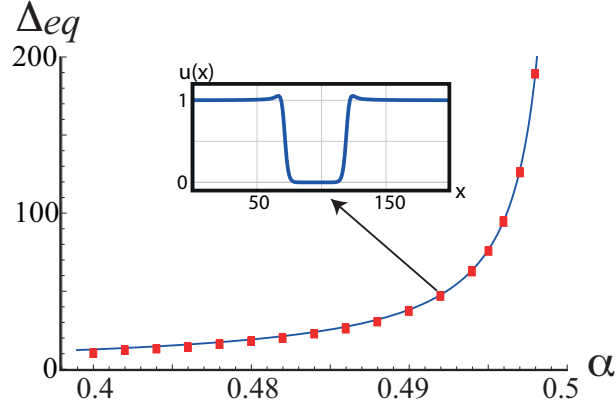
Figure 5: (Color online) Width of a fairy circle, as a function of aridity α in one dimension. The solid line represents the analytical prediction from Eq. (16). The squares are obtained by numerical simulations of Eq. (1). The inset is the spatial profile of biomass. Parameters are $\sigma = 0.8$, $n = 2$ and $\epsilon = 0.5$.

where

$$G(u_\pm, \sigma) = \left\langle \partial_x u_+ | u_+ \int_{-\infty}^{\infty} u^2(x', t) K(x' - x) dx' \right\rangle.$$

We neglect also the terms smaller than $1/\delta^{2n-1}$ in Eq. (13). Then, it is obtained

$$\partial_t \delta = \frac{3\sqrt{2}\epsilon N_n \sigma^n}{(n-1)(2\delta)^{n-1}} - \sqrt{2}\eta, \tag{14}$$

Strictly speaking, this equation of motion is quantitatively valid when $\partial_t \delta \sim \epsilon/\delta^{n-1} \sim \eta \ll 1$.

This result is valid for any power $n > 1$ in the Kernel function (2). We consider $n = 2$ and $N_n = 1/\pi\sigma$ in one dimension. Then, the equation (14) reads

$$\partial_t \Delta = \frac{6\sqrt{2}\epsilon\sigma}{\pi\Delta} - 2\sqrt{2}\left(\frac{1}{2} - \alpha\right), \tag{15}$$

where $\Delta = 2\delta$ is the width of the LS. The equilibrium width is given by

$$\Delta_{eq} = \frac{3\epsilon\sigma}{\pi\left(\frac{1}{2} - \alpha\right)}. \tag{16}$$

The linear stability analysis allows us to determine the eigenvalue $\lambda = -2\sqrt{2}\pi\eta^2/3\epsilon\sigma$. Therefore, for competitive interaction, i.e., $\epsilon > 0$, fairy circles are always stable.

We plot the width of the FC in one dimension as function of the aridity α in Figure 5. The width of localized structures grows as aridity increases. At the Maxwell point, i.e., $\alpha = 1/2$, the width of the fairy circle becomes infinite. In order to check the approximations used to derive the equilibrium size (16), we perform numerical simulations of Eq. (1). Both results are in good agreement, without any fitting parameter.

The fairy circles are observed in vast territories in southern Angola, Namibia, and South Africa [41, 42], where the annual rainfall ranges between 50 and 150 mm [49]. The size of FC increases from South to North where the climate becomes more and more arid [49]. The size can also be affected by the rainfall and nutrients [43]. Fairy circles average diameters varies in the range of 2 m-12 m [49]. In agreement with field observations, Fig. 5 shows indeed that the fairy circles diameter increases with the aridity.

Therefore, one-dimensional front interaction explains why the fairy circles size increase with the aridity. To wit, as environment aridity increases, the bare state becomes more and more favorable, increasing the fairy circles size. This mechanism demands, however, that the uniformly vegetated state must be always the most favorable one ($\alpha < 1/2$), otherwise the bare state propagates indefinitely. The same tendency is observed in two-dimensional simulations [34].

B.   Localized vegetation patch

In this subsection, we investigate the formation of a single localized patch that consist of a circular vegetated state surrounded by a bare state. This behavior occurs for high values of the aridity parameter, i.e., $\alpha > 1/2$. An example of a single localized patch is illustrated in Fig. 6. This localized solution corresponds to the counterpart of fairy circles.

Following a similar strategy than in the previous subsection (small ϵ and $\eta_f = \alpha - 1/2$), the patch width Δ in one spatial dimension obeys

$$\partial_t \Delta = \frac{6\sqrt{2}\epsilon N_n \sigma^n}{(n-1)(\Delta)^{n-1}} - 2\sqrt{2}\eta_f. \tag{17}$$

Note that, like in Eq. (14), the result obtain in Eq. (17) is generic for any n in (2). For $n = 2$, the stable vegetated patch have the size

$$\Delta_{eq} = \frac{3\epsilon\sigma}{\pi\left(\alpha - \frac{1}{2}\right)}. \tag{18}$$

The formula (18) is plotted in Fig. 7 by a solid line. Confrontation with direct numerical computation for the localized patch width is in good agreement, as shown in Fig. 7. There is no available data from the field observation to confirm this theoretical prediction.

C.   Bifurcation diagram

In this subsection, we establish the bifurcation diagram for both types of localized vegetation structures. We fix the length of the completion between plant σ, and we vary the degree of aridity α and the strength of the competitive interaction ϵ. We numerically establish a stability range of a single fairy circle and the localized patch in one dimensional setting. This analysis is summarized in the parameter plane (α, ϵ) of Fig. 8. For $\alpha < 1/2$, a single fairy circle is stable in the region FC as indicated in Fig.8. This stability region is bounded from below by dots and bounded from left by the Maxwell point $(\alpha = 1/2)$. Dynamically speaking, dots correspond to a saddle-node bifurcation. The parameter zone A indicates the regime where a FC shrinks and disappears. For large values of the strength of the
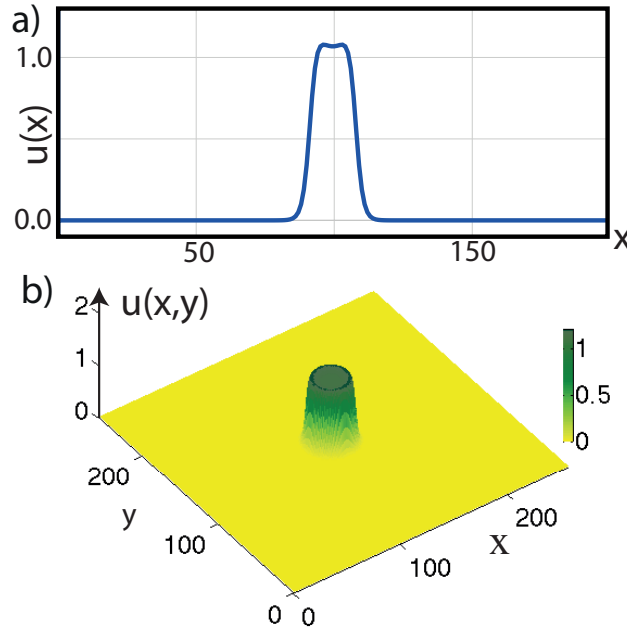

Figure 6: (Color online) Stationary localized patch obtained from numerical simulations of Eq. (1). (a) One dimension with $\alpha = 0.52$, $\sigma = 0.8$, $n = 2$ and $\epsilon = 0.5$. (b) Two dimensions with $\alpha = 0.56$, $\sigma = 0.1$, $n = 2.5$ and $\epsilon = 10$.
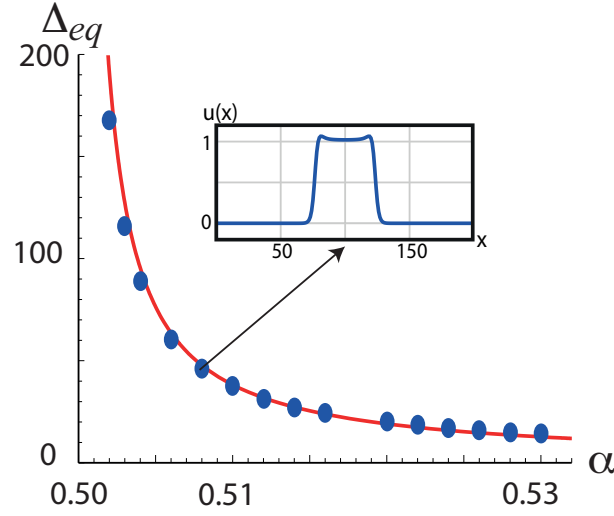
Figure 7: (Color online) Width of a localized vegetation patch, as a function of aridity α in one dimension. The solid line represents the analytical prediction from Eq. (18). The dots are obtained by numerical simulations of Eq. (1). The inset is the spatial profile of biomass. Parameters are $\sigma = 0.8$, $n = 2$ and $\epsilon = 0.5$.
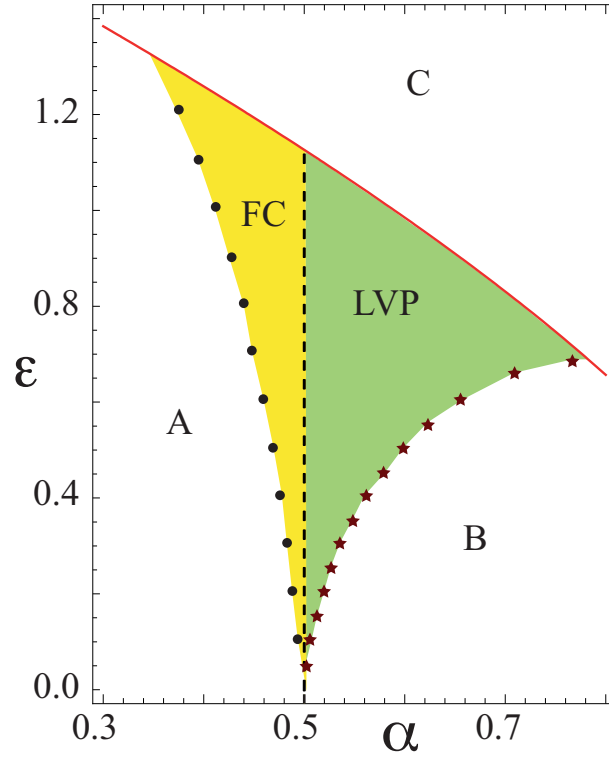

Figure 8: (Color online) Bifurcation diagram of localized structures for model Eq. (1), in parameter plane (α, ϵ), with $\sigma = 0.8$ and $n = 2$.

competition ϵ, the uniformly vegetated state becomes unstable with respect to symmetry breaking instability. The threshold associated with this instability is represented by a solid line. This line is obtained by plotting formula Eq. (5). This spatial instability impedes the existence of fairy circles in the region C, and may allow for the formation of periodic structures. For $\alpha > 1/2$, a single fairy grows until infinity and disappears, and a localized vegetation patch appears. This structure is stable in the region LVP, as shown in the bifurcation diagram of Fig. 8. The region B corresponds to a high degree of aridity. In this zone of parameters, a localized patch shrinks and disappears, and
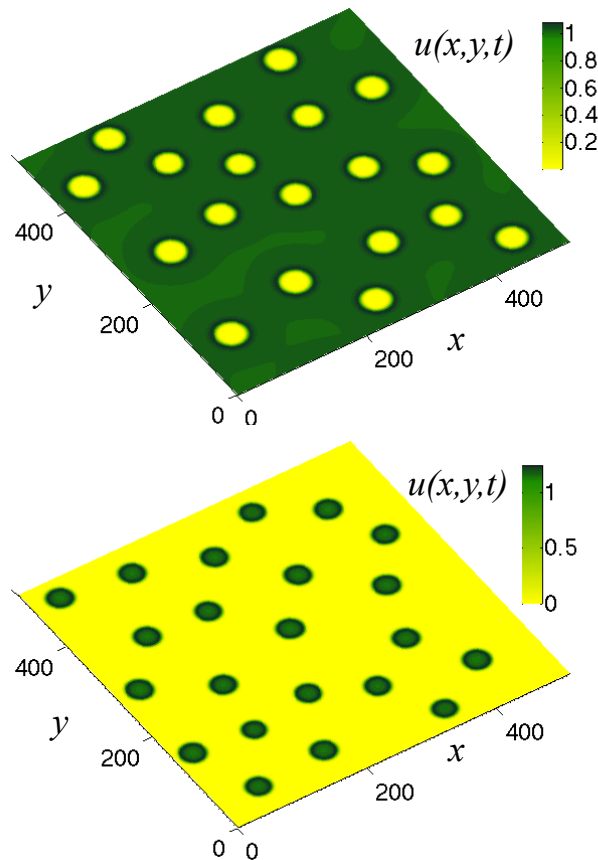
Figure 9: (Color online) Two dimensional localized vegetation patterns obtained from numerical simulations of Eq. (1). (a) Multi-fairy circles for $\alpha = 0.44$ (b) Multi-localized vegetation patches for $\alpha = 0.57$. Other parameters are $\sigma = 0.1$, $\epsilon = 10$ and $n = 2.5$.

transition toward a bare state occurs.

V. CONCLUSIONS

We have investigated the role of a strong nonlocal coupling in a bistable model namely the Nagumo model. This prototype model of population dynamics could be applied to vegetation dynamics. We have shown that far from any symmetry breaking or Turing type of instability, localized vegetation structures can be stabilized in large values of the aridity parameter. Their formation is attributed to the interaction between fronts mediated by a strong nonlocal coupling in the form of a Lorentzian. We have identified the following scenario: when increasing the level of the aridity, a large dip embedded in a uniformly vegetated state is formed. This structure has a single fringe peak that appeared in the spatial profile of the biomass. We have interpreted this behavior as a fairy circle. When increasing further the degree of aridity, localized vegetation patch can be formed in the system. This structure has a peak surrounded by the bare state. The localized structures reported in this work have a varying width as a function of aridity. In contrast, the width of localized vegetation structures found close to the symmetry breaking instability is determined by the most unstable Turing wavelength [26, 70]. We have established analytically a formula for the width of fairy circles and localized vegetation patches as a function the degree of aridity. The width of these localized structures is intrinsic to the dynamics of arid ecosystem and it is independent of external environmental effects, such as termites or ants. The results of direct numerical simulations of model Eq. (1) agreed with the analytical findings.

In this paper we have focused our analysis on a single localized structure, several of them could be stable as shown in the Fig. 9. The formation of multi-dips or peaks localized structures, their interactions and their stability are under investigation. Understanding the formation of localized structures is central not only in arid ecosystems but also in spatially extended out of equilibrium systems.

Acknowledgments

---

[1] H Leblond and D Mihalache, Physics Reports, **523**, 61 (2013).

[2] M. Tlidi, K. Staliunas, K. Panajotov, A.G. Vladimiorv, and M. Clerc, Localized structures in dissipative media: From Optics to Plant Ecology, Phil. Trans. R. Soc. A, **372**, 20140101 (2014).

[3] Y. Pomeau, Physica D **23**, 3 (1986); M. Tlidi, P. Mandel, and R. Lefever, Phys. Rev. Lett. **73**, 640 (1994); P. Coullet, C. Riera, and C. Tresser, Prog. Theor. Phys. Supp. **139**, (2000); M.G. Clerc and C. Falcon, Physica A **356**, 48 (2005); U. Bortolozzo, M. G. Clerc, C. Falcon, S. Residori, and R. Rojas, Phys. Rev. Lett. **96**, 214501 (2006); M. G. Clerc, E. Tirapegui, and M. Trejo, Phys. Rev. Lett. **97**, 176102 (2006); M. Tlidi and L. Gelens, Opt. Lett. **35**, 306 (2010); A.G. Vladimirov, R. Lefever, and M. Tlidi, Phys. Rev. A **84**, 043848 (2011); V. Skarka, N. B. Aleksic, M. Lekic, B. N. Aleksic, B. A. Malomed, D. Mihalache, and H. Leblond, Phys. Rev. A **90**, 023845 (2014).

[4] K. Staliunas and V.J. Sanchez-Morcillo, Physics Letters A **241**, 28 (1998); M. Tlidi, P. Mandel, R. Lefever, Phys. Rev. Lett. **81**, 979 (1998); H. Calisto, M. Clerc, R. Rojas, E. Tirapegui, Phys. Rev. Lett. **85**, 3805 (2000); M. Tlidi, P. Mandel, M. Le Berre, E. Ressayre, A. Tallet, and L. Di Menza, Opt. Lett. **25**, 487 (2000); D. Gomila, P. Colet, G. L. Oppo, and M. San Miguel, Phys. Rev. Lett. **87**, 194101 (2001); C. Chevallard, M. Clerc, P. Coullet, and J.-M. Gilli, Europhys. Lett. **58**, 686 (2002).

[5] U Bortolozzo, M.G. Clerc, and S Residori, New J. Phys. **11**, 093037 (2009).

[6] D. Escaff, Eur. Phys. J. D **62**, 33 (2011).

[7] P. Kolodner, D. Bensimon, and C. M. Surko, Phys. Rev. Lett. **60**, 1723 (1988); O. Thual, and S. Fauve, J. Phys. France **49**, 1829 (1988); B. A. Malomed, and A. Nepomnyashchy, , Phys. Rev. A **42**, 6009 (1990); W. Barten, M. Lücke, and M. Kamps, Phys. Rev. Lett. **66**, 2621 (1991); H. Riecke, Phys. Rev. Lett. **68**, 301 (1992); M. Dennin, G. Ahlers, and D. S. Cannell, Science **272**, 388 (1996); P. B. Umbanhowar, F. Melo, ans H. L. Swinney, Nature **382**, 793 (1996); H. Riecke, and G. D. Granzow, Phys. Rev. Lett. **81**, 333 (1998); C. Crawford, and H. Riecke, Physica D: Nonlinear Phenomena, **129**, 83 (1999).

[8] E. Hernandez-Garcia and C. Lopez, Physica D: Nonlinear Phenomena, **199**, 223 (2004).

[9] J.D. Murray, Mathematical Biology (Springer-Verlag, Berlin,1989).

[10] Shigui Ruan, Mathematics for Life Science and Medicine Biological and Medical Physics (Biomedical Engineering, Springer, 2007). Editors Y. Takeuchi, Y. Iwasa, and K. Sato.

[11] Y. Kuramoto, D. Battogtokh, and H. Nakao, Phys. Rev. Lett., **81**, 3543 (1998).

[12] S.I. Shima and Y. Kuramoto, Phys. Rev. E **69**, 036213 (2004).

[13] M. G. Clerc, D. Escaff, and V. M. Kenkre, Phys. Rev. E **72**, 056217 (2005); Phys. Rev. E **82**, 036210 (2010).

[14] D. Escaff, Int. J. Bif. Chaos **19**, 3509 (2009).

[15] M. Hernandez, D. Escaff, and R. Finger, Phys. Rev. E **85**, 056218 (2012).

[16] Wiesaw Krolikowski, and Ole Bang, Phys. Rev. E **63**, 016610 (2000).

[17] W. Krolikowski, O. Bang, J.J. Rasmussen, and J. Wyller, Phys. Rev. E **64**, 016612 (2001).

[18] O. Bang, W. Krolikowski, J. Wyller, and J.J. Rasmussen, Phys. Rev. E **66**, 046619 (2002).

[19] Y.V. Kartashov, L. Torner, V.A. Vysloukh, and D. Mihalache, Opt. Lett. **31**, 1483 (2006).

[20] D. Mihalache, D. Mazilu , F. Lederer, L.C. Crasovan, Y.V. Kartashov, L. Torner, and B.A. Malomed, Phys. Rev. E **74**, 066614 (2006).

[21] Y.J. He, B.A. Malomed, D. Mihalache, and H.Z. Wang, Phys. Rev. A **77**, 043826 (2008).

[22] L. Gelens, G. Van der Sande, P. Tassin, M. Tlidi, P. Kockaert, D. Gomila, I. Veretennicoff, and J. Danckaert, Phys. Rev. A **75**, 063812 (2007).

[23] I. Aranson and L. Tsimring, Granular Patterns, Oxford University Press, New York, 2009.

[24] R. Lefever and O. Lejeune, Bulletin of Mathematical biology, **59**, 263 (1997).

[25] O. Lejeune and M. Tlidi, Journal of Vegetation Science, **10**, 201 (1999).

[26] M. Tlidi, R. Lefever, and A. Vladimirov, Lect. Notes. Phys. **751**, 381 (2008).

[27] E. Gilad, J. von Hardenberg, A. Provenzale, M. Shachak, and E. Meron, Phys. Rev. Lett. **93**, 098105 (2004).

[28] P. Couteron, F. Anthelme, M.G. Clerc, D. Escaff, C. Fernandez-Oto, and M. Tlidi, Phil. Trans. R. Soc. **372**, 20140102 (2014).

[29] W. van Saarloos and P. C. Hohenberg, Physica D **56**, 303 (1992).

[30] L. Gelens, D. Gomila, G. Van der Sande, M.A. Matías, and P. Colet, Phys. Rev. Lett. **104**, 154101 (2010).

[31] P. Colet, M.A. Matías, L. Gelens, and D. Gomila, *Phys. Rev. E* **89**, 012914 (2014).

[32] L. Gelens, M.A. Matías, D. Gomila, T. Dorissen, and P. Colet, *Phys. Rev. E* **89**, 012915 (2014).

[33] C. Fernandez-Oto, M. G. Clerc, D. Escaff, and M. Tlidi, Phys. Rev. Lett. **110**, 174101 (2013).

[34] C. Fernandez-Oto, M. Tlidi, D. Escaff, and M. G. Clerc, Phil. Trans. R. Soc. A **372**, 20140009 (2014).

[35] R. E. Goldstein, G. H. Gunaratne, L. Gil, and P. Coullet, Phys. Rev. A **43**, 6700 (1991).

[36] X. Hutsebaut, C. Cambournac, M. Haelterman, J. Beeckman, and K. Neyts, JOSA B **22**, 1424 (2005)
[37] J.F. Henninot, J.F. Blach, and M. Warenghem, J. Opt. A **9**, 20 (2007).
[38] A. Minovich, D.N. Neshev, A. Dreischuh, W.Krolikowski, and Y.S. Kivshar, Opt. Lett. **32**, 1599 (2007).
[39] H.F. Howe and L.C. Westley, Plant Ecology, Second Edition, 1986, Chapter 9. Ecology of Pollination and Seed Dispersal
[40] L. Fraley, Environmental and Experimental Botany, **27**, 193 (1987).
[41] C. Albrecht , J.J. Joubert, and P.H. De Rycke, South Afican Journal of Science **97**, 23 (2001).
[42] T. Becker and S. Getzin, Basic and Applied Ecology, **1**, 149 (2000).
[43] M.D. Cramer and N.N. Barge, *PLoS ONE* **8**, e70876 (2013).
[44] M.D. Picker and V. Ross-Gillespie, K. Vlieghe, and E. Moll, Ecological Entomology **37**, 33 (2012).
[45] W.J. Jankowitz, M.W. Van Rooyen, D. Shaw, J.S. Kaumba, and N. van Rooyen, South African Journal of Botany, **74**, 332 (2008).
[46] Y. Naude, M.W. van Rooyen, and E.R. Rohwer, J. Arid Environ. **75**, 446 (2011).
[47] N. Juergens, Science **339**, 1618 (2013).
[48] S. Grube S, Basic and Applied Ecology, **3**, 367 (2002).
[49] M.W. van Rooyen, G.K. Theron, N. van Royen, W.J. Jankowitz, and W.K. Matthews, Journal of Arid Environments **57**, 467 (2004).
[50] R. Lefever and J.W. Turner, Comptes Rendus Mécanique, **340**, 818 (2012).
[51] R. Martínez-García, J.M. Calabrese, E. Hernandez-Garcia, and C. Lopez, Geophysical Research Letters, **40**, 6143 (2013).
[52] C.A. Klausmeier, Science **284**, 1826 (1999).
[53] J. von Hardenberg, E. Meron, M. Shachak, and Y. Zarmi, Phys. Rev. Lett. **87**, 198101 (2001).
[54] R. HilleRisLambers, M. Rietkerk, F. van den Bosch, H.H.T. Prins, and H. de Kroon, Ecology, **82**,50 (2001).
[55] T. Okayasu and Y. Aizawa, Prog. Theor. Phys. **106** 705 (2001).
[56] J.A. Sherratt, J. Math. Biol. **51**, 183 (2005).
[57] Weiming Wang, Quan-Xing Liu, and Zhen Jin, Phys. Rev. E **75**, 051913 (2007).
[58] S. Kefia, M. Rietkerka, M. van Baalenb, and M. Loreauc, Theoretical Population Biology, **71**, 367 (2007).
[59] P. D'Odorico, F. Laio, and L. Ridolfi, Journal of Geophysical Research: Biogeosciences, **111**, 2156 (2006).
[60] P. D'Odorico, F. Laio, A. Porporato, L. Ridolfi, and N. Barbier, Journal of Geophysical Research: Biogeosciences (2005-2012), **11**, G02021(2007).
[61] F. Borgogno, P. D'Odorico, F. Laio, and L. Ridolfi, Rev. Geophys. **47**, RG1005 (2009).
[62] L. Ridif, P. D'Odorici, and F. Laio, Noise induced phenomena in the environmental sciences (Cambridge University Press, 2011).
[63] R. Lefever, N. Barbier, P. Couteron, and O. Lejeune, Journal of Theoretical Biology **261**, 194 (2009).
[64] P. Coullet, Int. J. Bif. and Chaos, **12**, 2445 (2002).
[65] O. Lejeune, M. Tlidi, and P. Couteron, Phys. Rev. E **66**, 010901 (2002).
[66] M. Rietkerk, S.C. Dekke, P.C. de Ruiter, and J. van de Koppel, *Science* **305**, 1926 (2004).
[67] E. Meron, E. Gilad, J. von Hardenberg, M. Shachak, and Y. Zarmi, Chaos, Solitons and Fractals, **19**, 367 (2004).
[68] E. Meron, H. Yizhaq, and E. Gilad, Chaos **17**, 037109 (2007).
[69] E. Sheffera, H. Yizhaqa, M. Shachaka, and E. Meron, Journal of Theoretical Biology, **273**, 138 (2011).
[70] S. Getzin, K. Wiegand, T. Wiegand, and H. Yizhaq, J. von Hardenberg, and E. Meron, Ecography, **37**, 001 (2014).